Anisotropic exciton transport in transition-metal dichalcogenides

Areg Ghazaryan,[1] Mohammad Hafezi,[2,3,4] and Pouyan Ghaemi[1,5]
[1]*Department of Physics, City College, City University of New York, New York 10031, USA*
[2]*Joint Quantum Institute, NIST and University of Maryland, College Park, Maryland 20742, USA*
[3]*Department of Electrical Engineering and IREAP, University of Maryland, College Park, Maryland 20742, USA*
[4]*Department of Physics, College Park, Maryland 20742, USA*
[5]*Department of Physics, Graduate Center, City University of New York, New York 10016, USA*

(Received 15 April 2018; revised manuscript received 31 May 2018; published 14 June 2018)

In monolayer transitional metal dichalcogenides, the two excitonic states which are eigenstates of Coulomb interaction are coherent superposition of electron and holes in the two valleys. The exciton band which couples to the transverse electric mode of light has parabolic dispersion for the center-of-mass momentum, whereas the one which couples to the transverse magnetic mode has both parabolic and linear components. In this paper we show that the signatures of this band structure of excitons can be observed in exciton diffusion experiments. In particular, it is demonstrated that by pumping the system with linearly polarized light the exciton transport is anisotropic compared to circularly polarized pump and that such anisotropy is absent for the cases of two linearly or two quadratically dispersing bands. We show that the results persist for the moderate level of disorder present in realistic systems. Finally, we demonstrate that similar effects can be obtained for positively detuned exciton polaritons, in less stringent experimental requirements compared to the bare exciton case.

DOI: 10.1103/PhysRevB.97.245411

I. INTRODUCTION

Graphene, a single layer of graphite, has been the subject of intense research for over a decade due its true two-dimensional (2D) nature and its Dirac-type electronic bands arising from its honeycomb lattice structure [1,2]. The main obstacle for utilizing graphene in optoelectronics is the gapless nature of its electronic bands, which is protected by inversion symmetry. Numerous methods have been proposed to brake inversion symmetry of graphene and open a band gap at Dirac points [3]. Nevertheless, the gap obtained with these methods is usually small and not suitable for near-infrared or visible light experiments. Observation of a direct band gap in monolayer transition-metal dichalcogenides (TMDs) [4–6], such as MoS_2,$MoSe_2$,WS_2,WSe_2, with the size of the order of visible light frequency opened new avenues in this regard. In TMDs, the transition-metal atom is coordinated with six chalcogen atoms in trigonal prismatic geometry. The lattice structure of TMDs is similar to graphene, but the inversion symmetry is explicitly broken due to the alternating metal and chalcogen atoms. TMDs possess a gap in the range of 1.4–1.7 eV [7] and due to their 2D nature, which suppresses the screening of the charges, they host strongly bonded excitons [8–12]. The binding energy reaches up to 500 meV, therefore excitonic-related phenomena can be realized at room temperatures in these materials. Similar to graphene, the low energy band structure of TMDs consists of two degenerate valleys at the corners of the hexagonal Brillouin zone (BZ). Since Berry curvature has the opposite sign for the two valleys, right and left circularly polarized light selectively excites the electron-hole pairs in one of the two valleys [7]. Another important distinction of TMDs with graphene is the presence of strong spin-orbit coupling (SOC) originating from transition metal d bands, which polarizes the spin direction at the top of the valence band in each valley [7]. There is also spin splitting due to the SOC in the conduction band [13]. These correlations between valley and spin can be utilized for realizing both valley and spin coherence, which was demonstrated experimentally both in low and room temperatures [14–17].

Exciton-polariton (EP) [18–20] states are also extensively studied in TMDs. EPs are hybrid quasiparticles comprising exciton and photon, which are realized when the system is placed at the antinode of the planar optical cavity. Due to the spatial spreading of the photon, EPs have larger coherence length in comparison with excitons and are therefore, less susceptible to disorder scattering [21]. Since the masses of the exciton and photon are very different, by changing the cavity detuning the effective mass of polariton can be largely modified. In addition, the exciton part of polariton results in enhancement of polariton-polariton interaction. These characteristics show their signatures in physical phenomena such as the optical spin Hall effect [22–24] and Bose-Einstein condensation of polariton liquid [25–27]. Due to the strong light-matter coupling in TMDs, EPs have been successfully realized both in low and room temperatures [28–30]. Enhanced valley coherence of EPs compared to bare excitons in TMDs has been also demonstrated [31–33].

It is well established theoretically that due to the exchange interaction between electrons and holes in the two valleys, the exciton bound states with finite center-of-mass (CM) momentum are symmetric and antisymmetric superpositions of excitons in the two valleys [34–38]. The lower energy exciton band disperses quadratically whereas the higher energy band disperses linearly [Fig. 1(a)] [35–38]. The two bands are degenerate at zero CM momentum and couple to the transverse electric (TE) and transverse magnetic (TM) components of

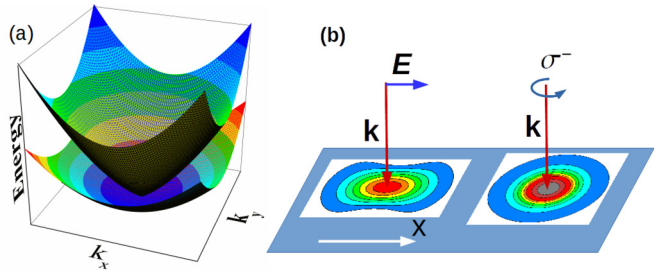

FIG. 1. (a) Schematic drawing of the band structure of excitons in TMDs and (b) depiction of exciton transport when the system is pumped with linearly polarized light (left) and right circularly polarized light (right).

light, respectively. This nontrivial excitonic band structure is not experimentally verified yet.

In this work we propose a method to observe the signatures of the novel form of the exciton dispersion through anisotropic exciton transport. Particularly, we demonstrate that when the system is excited with linearly polarized light, the nonpolarized emission is anisotropic, whereas it becomes isotropic for the circularly polarized pump [Fig. 1(b)]. This anisotropic transport is robust against moderate levels of disorder potential. We also analyze the transport phenomenon for EPs and show that similar anisotropic effect can be observed also for considerably positively detuned EPs. We show that the enhanced Coulomb interaction in TMDs, in comparison with III-V and II-VI semiconductor quantum well systems, which leads to larger velocity of excitons with small CM momentum, makes it possible to observe the signature of novel excitonic dispersion in transport measurements.

There were several attempts to experimentally probe exciton transport in TMDs using transient absorption microscopy [39,40], the direct charge-coupled device imaging method [41], spatially resolved steady-state, and time-resolved photoluminescence [42,43]. Obtained experimental results were analyzed using the 2D diffusion equation [40,41], which gives consistent results with the experiments for non-polarization-resolved transport dynamics. In these experiments both excitation and detection are not polarization resolved and the system is pumped with much larger energy compared to the exciton resonance. On another front, polarization-resolved transport of EPs with polarization beats appearing at specific directions has been experimentally demonstrated for the AlGaAs quantum well with the pulsed laser pump [44]. Our results show that such measurements on TMDs would reveal much more information about the strong particle-hole interactions which lead to the formation of excitons. Recent advancements in the quality of TMD samples shows the promise for experimental realization of our predictions.

The paper is organized as follows: In Sec. II we present effective Hamiltonians for calculating exciton and EP dispersions. We also discuss time-dependent Schrödinger equations resulting from effective Hamiltonians and the numerical procedure for simulating the transport dynamics of the excitons and EPs. In Sec. III we present the results derived from the framework outlined in Sec. II and discuss the potential application of the system to develop optical switches. Finally, we present the concluding remarks in Sec. IV.

II. THE MODEL HAMILTONIAN

Due to the strong binding of electrons and holes in excitons in TMDs, it is natural to study the dynamics of exciton as an individual quasiparticle. The exciton dispersion is obtained by solving the Bethe-Salpeter equation for the electron-hole pair [35,45] or alternatively, by the $\mathbf{k}\cdot\mathbf{p}$ perturbation method of the electron-hole pair Hamiltonian projected into the bands involved in optical transition [46,47]. It was shown that, due to the true 2D nature of TMDs and reduced screening of Coulomb interaction, the effect of exchange interaction is more pronounced [34–38] compared to III-V and II-VI semiconductor quantum well systems [48–51]. This excitonic band structure, for small center-of-mass momenta, can be expressed using the following effective Hamiltonian:

$$\mathcal{H}_{\rm ex}(\mathbf{k}) = \begin{pmatrix} h_{\rm ex}(\mathbf{k}) & S^-_{\rm ex}(\mathbf{k}) \\ S^+_{\rm ex}(\mathbf{k}) & h_{\rm ex}(\mathbf{k}) \end{pmatrix}, \tag{1}$$

where $\mathbf{k} = |\mathbf{k}|e^{i\varphi}$, $h_{\rm ex}(\mathbf{k}) = E^0_{\rm ex} + \frac{\hbar^2|\mathbf{k}|^2}{2m_{\rm ex}} + \alpha|\mathbf{k}|$, $S^\pm_{\rm ex}(\mathbf{k}) = \alpha|\mathbf{k}|e^{\pm i2\varphi}$. Here $E^0_{\rm ex}$ corresponds to the energy of the exciton at $\mathbf{k}=0$ measured from the top of the valence band. In the numerical calculation we use the value $m_{\rm ex} = 0.6m_0$ (m_0 being free electron mass) for exciton effective mass. The $\alpha = 90$ meV nm is proportional to the amplitude of exchange interaction [35] and, due to stronger Coulomb interaction in TMDs, it is two orders of magnitude larger than the value in III-V and II-VI semiconductor quantum well systems [48,49,51]. The enhanced value of exciton velocity at low momenta in TMDs is particularly important for the experimental realization of our results. The two spinor components of the states that Hamiltonian (1) act on correspond to the two valleys or spins of the constituent electron hole of exciton. As was noted above optical transitions in each valley couple to specific circular polarization of light, therefore, the Hamiltonian (1) is effectively presented in the circular polarization basis. Hamiltonian (1) has two eigenvalues, the lowest in energy having parabolic dispersion $E^1_{\rm ex}(\mathbf{k}) = E^0_{\rm ex} + \frac{\hbar^2|\mathbf{k}|^2}{2m_{\rm ex}}$, while the higher one has both linear and parabolic components $E^2_{\rm ex}(\mathbf{k}) = E^0_{\rm ex} + 2\alpha|\mathbf{k}| + \frac{\hbar^2|\mathbf{k}|^2}{2m_{\rm ex}}$. It can be shown that the lower band couples to the TE and the upper one to TM linearly polarized light [35].

The Hamiltonian describing EPs can be written as the exciton-photon coupled system [52],

$$\mathcal{H}_{\rm ep}(\mathbf{k}) = \begin{pmatrix} h_{\rm ex}(\mathbf{k}) & S^-_{\rm ex}(\mathbf{k}) & V & 0 \\ S^+_{\rm ex}(\mathbf{k}) & h_{\rm ex}(\mathbf{k}) & 0 & V \\ V & 0 & h_{\rm p}(\mathbf{k}) & S^-_{\rm p}(\mathbf{k}) \\ 0 & V & S^+_{\rm p}(\mathbf{k}) & h_{\rm p}(\mathbf{k}) \end{pmatrix}, \tag{2}$$

where the photon has a parabolic dispersion $h_{\rm p}(\mathbf{k}) = E^0_{\rm p} + \frac{\hbar^2|\mathbf{k}|^2}{2m_{\rm p}}$ with effective mass $m_{\rm p} = 4\times10^{-5}m_0$. The nondiagonal term in the photon part of the Hamiltonian $S^\pm_{\rm p}(\mathbf{k}) = \beta|\mathbf{k}|^2e^{\pm i2\varphi}$ (with double winding and amplitude $\beta = 47300$ meV nm^2) is due to the TE-TM splitting [53]. Coupling amplitude between exciton and photon parts of Hamiltonian (2) is proportional to Rabi frequency Ω by $V = \hbar\Omega/2$ and $\hbar\Omega = 20$ meV. The detuning of the EP system is $\Delta = E^0_{\rm p} - E^0_{\rm ex}$. The Hamiltonian (2) has four eigenvalues, two of which inherit the linear

component of dispersion from the excitonic component. As will be discussed below, the observation of the linear component of EP dispersion depends strongly on detuning.

In order to calculate the spatial dynamics of excitons we numerically solve time-dependent Schrödinger equation corresponding to the Hamiltonian (1), namely

$$\begin{aligned} i\hbar\frac{\partial\phi_R(\mathbf{r},t)}{\partial t} &= h_{\rm ex}(\mathbf{k})\phi_R(\mathbf{r},t) + S^-_{\rm ex}(\mathbf{k})\phi_L(\mathbf{r},t) \\ &\quad - \frac{i\hbar}{2\tau_{\rm ex}}\phi_R(\mathbf{r},t) + U(\mathbf{r})\phi_R(\mathbf{r},t) + P_R(\mathbf{r}), \\ i\hbar\frac{\partial\phi_L(\mathbf{r},t)}{\partial t} &= h_{\rm ex}(\mathbf{k})\phi_L(\mathbf{r},t) + S^+_{\rm ex}(\mathbf{k})\phi_R(\mathbf{r},t) \\ &\quad - \frac{i\hbar}{2\tau_{\rm ex}}\phi_L(\mathbf{r},t) + U(\mathbf{r})\phi_L(\mathbf{r},t) + P_L(\mathbf{r}), \end{aligned} \tag{3}$$

where $\phi_R(\mathbf{r},t)$ and $\phi_L(\mathbf{r},t)$ correspond to exciton wave functions in two valleys. The double winding of $S^{\pm}_{\rm ex}(\mathbf{k})$ accounts for the orbital momentum difference between right and left circularly polarized light. $\tau_{\rm ex} = 5.3$ ps is the exciton lifetime (extracted from time-resolved photoluminescence measurement) [29,32], $U(\mathbf{r})$ is the disorder potential acting on the excitons and $P_R(\mathbf{r})$ and $P_L(\mathbf{r})$ are the continuous-wave (cw) pump terms for right and left circular polarization, respectively. The exciton disorder potential is assumed to have Gaussian correlation in space [21,54,55],

$$\langle U(\mathbf{r})U(\mathbf{r}')\rangle = \sigma^2 e^{-|\mathbf{r}-\mathbf{r}'|^2/\xi^2}, \tag{4}$$

where we consider the correlation length $\xi = 10$ nm and σ is the correlation amplitude. After discretization of the space the disorder potential can be calculated using the formula,

$$U(\mathbf{r}) = \frac{2\sigma\sqrt{\Delta x\Delta y}}{\xi\sqrt{\pi}}\sum_{\mathbf{r}'} c(\mathbf{r}')e^{-2|\mathbf{r}-\mathbf{r}'|^2/\xi^2}, \tag{5}$$

where $\langle c(\mathbf{r})c(\mathbf{r}')\rangle = \delta_{\mathbf{r}\mathbf{r}'}$ and Δx, Δy denote discretization steps in x and y directions, respectively. We model the pump by the Gaussian shape in momentum space [23,56],

$$P_{R,L}(\mathbf{k},t) = P^0_{R,L}e^{-(\mathbf{k}-\mathbf{k}_p)^2L^2/4}\frac{i\Gamma e^{-iE_pt/\hbar}}{h_{\rm ex}(\mathbf{k}) - E_p - i\Gamma}, \tag{6}$$

where $\mathbf{k}_p$ is the pump momentum, E_p is the pump energy, Γ is the linewidth, and L the pump spot size. We take pump energy E_p to be the zero energy of the system in order to make the pump term time independent.

A similar time-dependent Schrödiner equations can be written for polaritons:

$$\begin{aligned} i\hbar\frac{\partial\psi(\mathbf{r},t)}{\partial t} &= h_{\rm p}(\mathbf{k})\psi(\mathbf{r},t) + S_{\rm p}(\mathbf{k})\psi(\mathbf{r},t) \\ &\quad - \frac{i\hbar}{2\tau_p}\psi(\mathbf{r},t) + V\phi(\mathbf{r},t) + P(\mathbf{r}), \\ i\hbar\frac{\partial\phi(\mathbf{r},t)}{\partial t} &= h_{\rm ex}(\mathbf{k})\phi(\mathbf{r},t) + S_{\rm ex}(\mathbf{k})\phi(\mathbf{r},t) \\ &\quad - \frac{i\hbar}{2\tau_{\rm ex}}\phi(\mathbf{r},t) + V\psi(\mathbf{r},t) + U(\mathbf{r})\phi(\mathbf{r},t), \end{aligned} \tag{7}$$

where now $\psi(\mathbf{r},t)$ and $\phi(\mathbf{r},t)$ are two component spinors (denoting the two valleys or two circular polarizations) corresponding to the wave function for the photon and exciton, respectively. $\tau_p = 1.3$ ps [20,32] is the photon lifetime in the cavity. In (7) the disorder potential is only acting on the exciton component of polariton and the pump is generating photons, which get converted into polaritons through exciton-photon coupling. In this case the pump term is also a spinor with two components denoting two circular polarizations of the pump.

We numerically solve (3) and (7) on a 256×256 grid in real space of the size 3 μm×3 μm. For the terms in the Hamiltonian which are diagonal in momentum space we Fourier transform the wave function from real space, calculate the action of those terms, and then transform back [52] using the fast Fourier transform algorithm [57]. The time step for integration of Eqs. (3) and (7) is $\Delta t = 10^{-4}$ ps and we run the simulation until the populations of the particles stabilize (around 40 ps). For integration we use the Adams-Bashforth-Moulton method [57] in the nVidia CUDA GPU framework.

III. RESULTS AND DISCUSSION

As was noted above one of the characteristics of the excitons in TMDs is the presence of the linear component in the dispersion of one of the excitonic bands. Since the EP is a superposition of the exciton and photon, it inherits this linear component of dispersion. Figure 2 shows the dependence of the two excitonic and two lower EP branches (for detunings $\Delta = 0, 20, 60$ meV) on absolute value of in-plane momentum $|\mathbf{k}|$. The momentum range presented in the figures corresponds to the range accessible in angle-resolved absorption and photoluminescence experiments on TMDs. As was noted above and can be seen from Fig. 2(a) one of the branches has linear dependence on momentum. Both exciton bands have also the parabolic term, which is extremely small for the values of momenta considered and consequently the lowest exciton branch appears to be flat. The main objective of the current work is to find experimental signature which will demonstrate

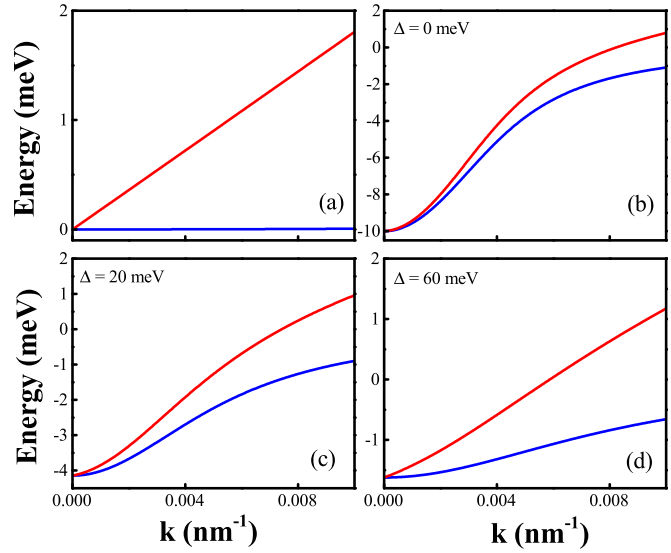

FIG. 2. The dependence of two exciton branches resulting from (1) (a) and lower two EP branches from (2) for detunings $\Delta = 0$ meV (b), $\Delta = 20$ meV (c), and $\Delta = 60$ meV (d) on absolute value of in plane momentum $|\mathbf{k}|$.

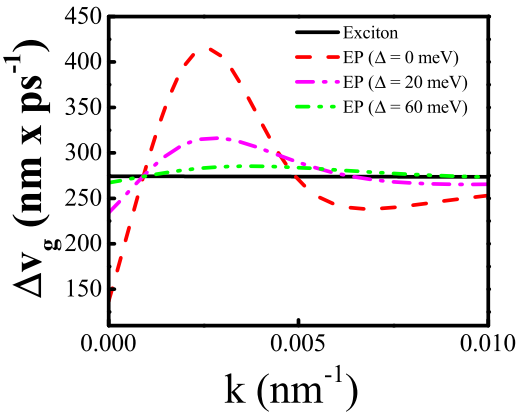

FIG. 3. The dependence of the difference of group velocities of two branches of exciton and EP shown in Fig. 2 on absolute value of in-plane momentum $|\mathbf{k}|$.

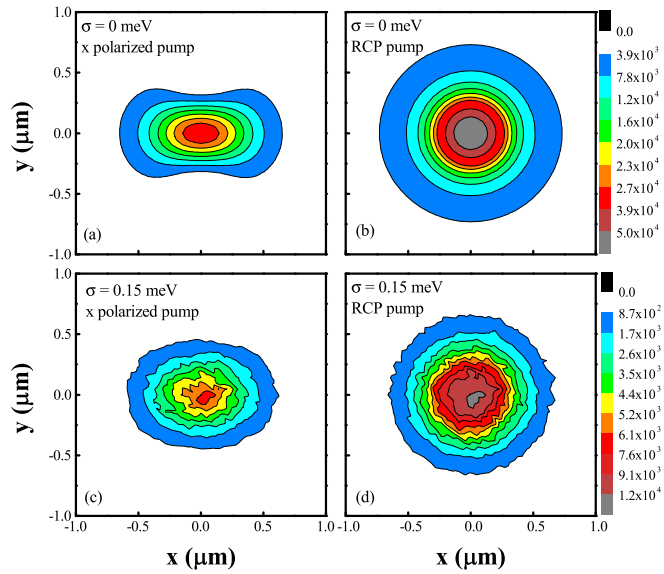

FIG. 4. Exciton transport when pumped with the x polarized pump (a) and (c) and right circularly polarized (RCP) pump (b) and (d). (a) and (b) These correspond to the case without disorder, (c) and (d) for the case with disorder with correlation amplitude $\sigma = 0.15\,\text{meV}$.

the presence of the linear component in exciton dispersion. In Figs. 2(b)–2(d) we also present two lower EP dispersions for different detuning. While the linear component is present in the upper energy branch for all values of detuning, it becomes pronounced only for large positive detuning ($\Delta = 60\,\text{meV}$). This is already an indication that using EPs in the current setup is not going to be as beneficial as is the case for other setups involving EP transport (such as the optical spin Hall effect [22,23]), because the features which are of our interest show up for EPs which comprise mostly the exciton component. This is related to the fact that photon has extremely small effective mass compared to the exciton and although the exciton has a linear component in its dispersion, for negative or close to zero detunings the photon component will prevail already at extremely small momenta, making the experimental observation of the linear component unrealistic due to the finite momentum broadening of the pump.

The essential difference between linear and parabolic bands which serves as a motivation for the experimental setup presented here is the difference between group velocities of two branches close to $\mathbf{k} = 0$ momentum. In Fig. 3 the dependence of the difference of group velocities ($v_g = \frac{1}{\hbar}\frac{\partial E(\mathbf{k})}{\partial \mathbf{k}}$) of two branches shown in Fig. 2 on the size of the in-plane momentum is presented. For the case of excitons the difference is constant $\Delta v_g = 2\alpha/\hbar \approx 274.3\,\text{nm/ps}$. As is evident in Fig. 2 for EPs the group velocity difference gets decreased for small momenta compared to exctions. The peak at $|\mathbf{k}| = 3\,\mu\text{m}^{-1}$ is due to the TE-TM splitting of cavity, which is parabolic. With the increase of the value of in-plane momentum $|\mathbf{k}|$ the EP becomes more excitonlike and the group velocity difference converges to the constant value for excitons.

In order to study large group velocity difference at small momenta due to the linear component of the dispersion we propose the exciton or EP transport experiment using the polarized pump similar to the experiment performed for the AlGaAs quantum well [44]. For the current setup polarization-resolved detection is not essential. Since the excitons have finite lifetime and group velocity difference due to the TE-TM splitting of the cavity prevails at intermediate momenta, the form and energy of the pump plays essential role in the current setup. It is clear that the pump should operate close to the minimum of two branches of excitons or lower EPs. In addition, for EPs it is desirable that the pump spot size be large enough, so that momentum broadening of the pump does not overlap with the TE-TM splitting dominated region of the group velocity difference. Finally, the finite lifetime of the exciton or EP poses the upper bound on the pump spot size, so that the transport anisotropy region manages to escape the pumping region and is detectable in the experiment. Therefore, we use the pump with parameters $E_p = E_{\text{ex}}^0$ [or equal to the lowest EP branch derived from $\mathcal{H}_{\text{ep}}(\mathbf{0})$], $\mathbf{k}_p = 0$, $\Gamma = 0.2\,\text{meV}$, $L = 400\,\text{nm}$, and $P^0 = 10^4$.

In Fig. 4 results of exciton transport are presented when the system is pumped with linearly polarized (x denoting the direction of linear pump polarization) and right circularly polarized (RCP) pumps. The emitted light is not polarization resolved. As can be seen from Fig. 4(a) for the x-polarized pump the obtained signal is anisotropic. As was mentioned above the fully parabolic branch of exciton couples to TE polarization, whereas the branch which has both linear and parabolic components couples to TM polarization of light. Therefore, when the system is pumped with x-polarized light it couples to the upper branch of excitons in the x direction and lower branch in the y direction. Since the upper branch has larger group velocity compared to the lower branch this results in observed anisotropy. At intermediate directions, the x-polarized light is not an eigenstate of the system and therefore, the polarization direction is rotated as excitons move away from the pumping spot due to the exchange interaction. The largest rotation happens at diagonal directions [44]. Therefore, at intermediate angles the distance of propagation depends on which proportion of its lifetime exciton is in the eigenstate of TM polarization. For the case of the RCP pump shown in Fig. 4(b), the signal is symmetric, because for all directions RCP light can be decomposed into TE and

TM components with equal amplitude. As a result the TM component is always present and dominates the propagation. It should be noted that we have considered other types of dispersions for excitons and anisotropic propagation is only present for this special case. In particular, in the initial work on TMD excitons [34], it was argued that the two excitons can be described with linear dispersions of Dirac massless particles. While it was later clarified that this calculation does not include intravalley exchange interaction [35,36,38], our current setup gives the possibility of experimentally probing the actual dispersion of excitons. When considering either gapless linear dispersions or parabolic dispersions for both of the two exciton branches the signal is always isotropic when the pump parameters described above has been used. As is shown in Figs. 4(c) and 4(d) the anisotropy is present also for the case of disorder with correlation amplitude $\sigma = 0.15$ meV. In current TMD samples disorder is quite strong and the transport is dominated by the disorder, which makes the observation of the presented anisotropic transport cumbersome. Despite that, recent advances in sample preparation and exciton diffusion measurement [43] bring the transport signatures presented in the current paper within experimental reach in upcoming years. Experimental observation of the propagation of Bloch surface wave polaritons in monolayer tungsten disulfide (WS_2) up to 42.2 μm [58] is also encouraging in this regard.

The anisotropic transport setup can also be used to set up optical switches without the need of entering the condensation regime [59–61]. In particular consider the initial RCP pump. As was noted above the propagation is isotropic in this case. Now consider the second pump at the same spot. If the second pump is again RCP and has the same phase as the initial one, the signal will not change. Whereas, if the second pump is left circularly polarized (LCP), then the sum of two pumps will be x linearly polarized and the signal will be anisotropic, which could be detected perpendicular to the overall pump polarization direction.

Finally, we discuss whether this effect can be observed for EPs. As was noted above the group velocity difference close to $k = 0$ drops down considerably with the decrease of detuning. The comparable group velocity difference to excitons can be obtained for the detuning $\Delta = 60$ meV. In this case at $\mathbf{k} = 0$ the proportion of the exciton component of EP is 97%, so the impact of the photon component should not be substantial. In Fig. 5 the results of EP transport are presented when the system is pumped with x polarized and RCP pumps as in Fig. 4. As can be seen from Fig. 5(a) anisotropic transport is observed for this case as well. Due to the photonic component of EPs, the overall group velocities have increased, so that the signal propagates at much longer distances than with excitons. This makes the observation of the signal less troublesome, because of the clear separation of the signal and pump regions. In terms of disorder scattering, the usage of EPs is preferred as well. This can be clearly seen in Figs. 5(c) and 5(d), where the anisotropy of the signal survives even for disorders with the correlation amplitude twice larger compared to the exciton (no transport anisotropy was observed for exciton transport at $\sigma = 0.3$ meV). Therefore, this clearly demonstrates that even though considerably positively detuned EPs should be used in the experiment to observe transport anisotropy, the usage of EPs could be preferred compared to the bare exciton system.

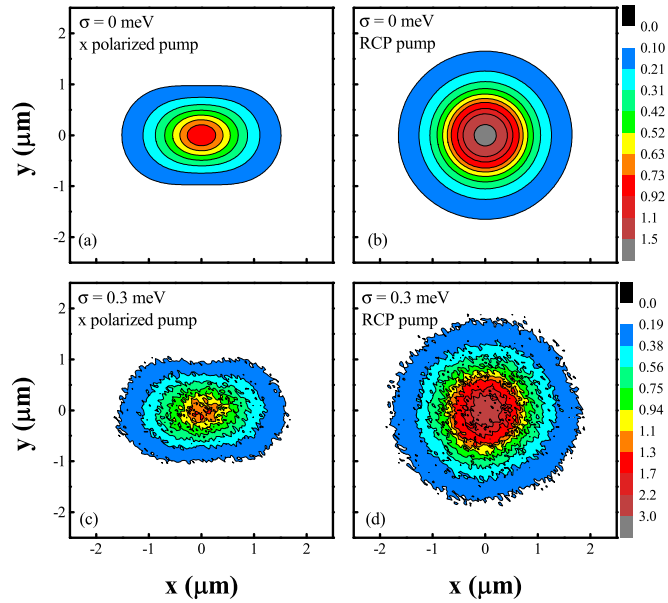

FIG. 5. EP transport when pumped with x-polarized pump (a) and (c), and right circularly polarized (RCP) pump (b) and (d). (a) and (b) Corresponding to the case without disorder, (c) and (d) for the case with disorder with correlation amplitude $\sigma = 0.3$ meV. The detuning of EPs in the calculations is $\Delta = 60$ meV.

IV. CONCLUSIONS

In conclusion we have presented a method to experimentally observe the unique structure of exciton dispersion in TMDs. In particular, we analyzed transport properties of excitons and EPs, when the system is pumped close to the bottom of the quasiparticle band. Pumping with the linearly polarized pump resulted in anisotropic photoemission compared to the circularly polarized pump. We showed that the effect is related to the large group velocity difference between two branches of quasiparticles due to the linear component of dispersion for one of the branches. We have analyzed the effect of disorder and showed that the results persist for the moderate levels of disorder in the system. Finally, we demonstrated that a similar effect should be present for positively detuned EPs as well. The usage of EPs in this regard is preferred over excitons, despite the fact that in considerably positively detuned EPs the photon proportion is small. Our results shows that upon the development of better quality samples, exciton and EP transport can be used to develop optical switches which does not require the realization of superfluid phases. Given the experimental observation of quantum coherent EPs in TMDs, even at room temperature, applications of EPs in these materials for development of quantum switches is particularly interesting and deserves further studies.

ACKNOWLEDGMENTS

We acknowledge fruitful conversations with Vinod Menon. This research was supported under National Science Foundation Grants No. EFRI-1542863, No. CNS-0958379, No. CNS-0855217, and No. ACI-1126113, and the City University of New York High Performance Computing Center at the College of Staten Island.

[1] A. H. Castro Neto, F. Guinea, N. M. R. Peres, K. S. Novoselov, and A. K. Geim, Rev. Mod. Phys. **81**, 109 (2009).

[2] M. O. Goerbig, Rev. Mod. Phys. **83**, 1193 (2011).

[3] E. McCann and M. Koshino, Rep. Prog. Phys. **76**, 056503 (2013).

[4] K. F. Mak, C. Lee, J. Hone, J. Shan, and T. F. Heinz, Phys. Rev. Lett. **105**, 136805 (2010).

[5] A. Splendiani, L. Sun, Y. Zhang, T. Li, J. Kim, C.-Y. Chim, G. Galli, and F. Wang, Nano Lett. **10**, 1271 (2010).

[6] X. Duan, C. Wang, A. Pan, R. Yu, and X. Duan, Chem. Soc. Rev. **44**, 8859 (2015).

[7] D. Xiao, G.-B. Liu, W. Feng, X. Xu, and W. Yao, Phys. Rev. Lett. **108**, 196802 (2012).

[8] G. Wang, A. Chernikov, M. M. Glazov, T. F. Heinz, X. Marie, T. Amand, and B. Urbaszek, Rev. Mod. Phys. **90**, 021001 (2018).

[9] T. C. Berkelbach, M. S. Hybertsen, and D. R. Reichman, Phys. Rev. B **88**, 045318 (2013).

[10] K. He, N. Kumar, L. Zhao, Z. Wang, K. F. Mak, H. Zhao, and J. Shan, Phys. Rev. Lett. **113**, 026803 (2014).

[11] C. Zhang, H. Wang, W. Chan, C. Manolatou, and F. Rana, Phys. Rev. B **89**, 205436 (2014).

[12] T. C. Berkelbach, M. S. Hybertsen, and D. R. Reichman, Phys. Rev. B **92**, 085413 (2015).

[13] A. Kormányos, G. Burkard, M. Gmitra, J. Fabian, V. Zólyomi, N. D. Drummond, and V. Fal'ko, 2D Mater. **2**, 022001 (2015).

[14] H. Zeng, J. Dai, W. Yao, D. Xiao, and X. Cui, Nat. Nanotechnol. **7**, 490 (2012).

[15] K. F. Mak, K. He, J. Shan, and T. F. Heinz, Nat. Nanotechnol. **7**, 494 (2012).

[16] T. Cao, G. Wang, W. Han, H. Ye, C. Zhu, J. Shi, Q. Niu, P. Tan, E. Wang, B. Liu, and J. Feng, Nat. Commun. **3**, 887 (2012).

[17] G. Wang, X. Marie, B. L. Liu, T. Amand, C. Robert, F. Cadiz, P. Renucci, and B. Urbaszek, Phys. Rev. Lett. **117**, 187401 (2016).

[18] V. Savona, C. Piermarocchi, A. Quattropani, P. Schwendimann, and F. Tassone, Phase Trans. **68**, 169 (1999).

[19] I. Carusotto and C. Ciuti, Rev. Mod. Phys. **85**, 299 (2013).

[20] H. Deng, H. Haug, and Y. Yamamoto, Rev. Mod. Phys. **82**, 1489 (2010).

[21] V. Savona, J. Phys.: Condens. Matter **19**, 295208 (2007).

[22] A. Kavokin, G. Malpuech, and M. Glazov, Phys. Rev. Lett. **95**, 136601 (2005).

[23] C. Leyder, M. Romanelli, J. P. Karr, E. Giacobino, T. C. H. Liew, M. M. Glazov, A. V. Kavokin, G. Malpuech, and A. Bramati, Nat. Phys. **3**, 628 (2007).

[24] I. A. Shelykh, A. V. Kavokin, Y. G. Rubo, T. C. H. Liew, and G. Malpuech, Semicond. Sci. Technol. **25**, 013001 (2010).

[25] J. Kasprzak, M. Richard, S. Kundermann, A. Baas, P. Jeambrun, J. M. J. Keeling, F. M. Marchetti, M. H. Szymanska, R. Andre, J. Staehli, V. Savona, P. B. Littlewood, B. Deveaud, and L. S. Dang, Nature (London) **443**, 409 (2006).

[26] R. Balili, V. Hartwell, D. Snoke, L. Pfeiffer, and K. West, Science **316**, 1007 (2007).

[27] Y. Sun, P. Wen, Y. Yoon, G. Liu, M. Steger, L. N. Pfeiffer, K. West, D. W. Snoke, and K. A. Nelson, Phys. Rev. Lett. **118**, 016602 (2017).

[28] X. Liu, T. Galfsky, Z. Sun, F. Xia, E.-c. Lin, Y.-H. Lee, S. Kéna-Cohen, and V. M. Menon, Nat. Photon. **9**, 30 (2015).

[29] S. Dufferwiel, S. Schwarz, F. Withers, A. A. P. Trichet, F. Li, M. Sich, O. Del Pozo-Zamudio, C. Clark, A. Nalitov, D. D. Solnyshkov, G. Malpuech, K. S. Novoselov, J. M. Smith, M. Skolnick, D. N. Krizhanovskii, and A. I. Tartakovskii, Nat. Commun. **6**, 8579 (2015).

[30] S. Wang, S. Li, T. Chervy, A. Shalabney, S. Azzini, E. Orgiu, J. A. Hutchison, C. Genet, P. Samorì, and T. W. Ebbesen, Nano Lett. **16**, 4368 (2016).

[31] Z. Sun, J. Gu, A. Ghazaryan, Z. Shotan, C. R. Considine, M. Dollar, B. Chakraborty, X. Liu, P. Ghaemi, S. Kéna-Cohen, and V. M. Menon, Nat. Photon. **11**, 491 (2017).

[32] S. Dufferwiel, T. P. Lyons, D. D. Solnyshkov, A. A. P. Trichet, F. Withers, S. Schwarz, G. Malpuech, J. M. Smith, K. S. Novoselov, M. S. Skolnick, D. N. Krizhanovskii, and A. I. Tartakovskii, Nat. Photon. **11**, 497 (2017).

[33] Y.-J. Chen, J. D. Cain, T. K. Stanev, V. P. Dravid, and N. P. Stern, Nat. Photon. **11**, 431 (2017).

[34] H. Yu, G.-B. Liu, P. Gong, X. Xu, and W. Yao, Nat. Commun. **5**, 3876 (2014).

[35] D. Y. Qiu, T. Cao, and S. G. Louie, Phys. Rev. Lett. **115**, 176801 (2015).

[36] F. Wu, F. Qu, and A. H. MacDonald, Phys. Rev. B **91**, 075310 (2015).

[37] T. Yu and M. W. Wu, Phys. Rev. B **89**, 205303 (2014).

[38] Y. N. Gartstein, X. Li, and C. Zhang, Phys. Rev. B **92**, 075445 (2015).

[39] Q. Cui, F. Ceballos, N. Kumar, and H. Zhao, ACS Nano **8**, 2970 (2014).

[40] L. Yuan, T. Wang, T. Zhu, M. Zhou, and L. Huang, J. Phys. Chem. Lett. **8**, 3371 (2017).

[41] T. Kato and T. Kaneko, ACS Nano **10**, 9687 (2016).

[42] S. Mouri, Y. Miyauchi, M. Toh, W. Zhao, G. Eda, and K. Matsuda, Phys. Rev. B **90**, 155449 (2014).

[43] F. Cadiz, C. Robert, E. Courtade, M. Manca, L. Martinelli, T. Taniguchi, K. Watanabe, T. Amand, A. C. H. Rowe, D. Paget, B. Urbaszek, and X. Marie, Appl. Phys. Lett. **112**, 152106 (2018).

[44] W. Langbein, I. Shelykh, D. Solnyshkov, G. Malpuech, Y. Rubo, and A. Kavokin, Phys. Rev. B **75**, 075323 (2007).

[45] M. Rohlfing and S. G. Louie, Phys. Rev. B **62**, 4927 (2000).

[46] G. E. Pikus and G. L. Bir, Zh. Eksp. Teor. Fiz. **60**, 195 (1971) [Sov. Phys. JETP **33**, 108 (1971)].

[47] G. L. Bir and G. E. Pikus, *Symmetry and Strain Induced Effects in Semiconductors* (Wiley, New York, 1975).

[48] L. C. Andreani and F. Bassani, Phys. Rev. B **41**, 7536 (1990).

[49] S. Jorda, U. Rössler, and D. Broido, Phys. Rev. B **48**, 1669 (1993).

[50] M. Z. Maialle, E. A. de Andrada e Silva, and L. J. Sham, Phys. Rev. B **47**, 15776 (1993).

[51] H. Tong and M. W. Wu, Phys. Rev. B **83**, 235323 (2011).

[52] O. Bleu, D. D. Solnyshkov, and G. Malpuech, Phys. Rev. B **96**, 165432 (2017).

[53] G. Panzarini, L. C. Andreani, A. Armitage, D. Baxter, M. S. Skolnick, V. N. Astratov, J. S. Roberts, A. V. Kavokin, M. R. Vladimirova, and M. A. Kaliteevski, Phys. Rev. B **59**, 5082 (1999).

[54] V. Savona and W. Langbein, Phys. Rev. B **74**, 075311 (2006).

[55] D. Sarchi, M. Wouters, and V. Savona, Phys. Rev. B **79**, 165315 (2009).

[56] T. C. H. Liew, C. Leyder, A. V. Kavokin, A. Amo, J. Lefrère, E. Giacobino, and A. Bramati, Phys. Rev. B **79**, 125314 (2009).

[57] W. H. Press, S. A. Teukolsky, W. T. Vetterling, and B. P. Flannery, *Numerical Recipes: The Art of Scientific Computing*, 3rd ed. (Cambridge University Press, New York, 2007).

[58] F. Barachati, A. Fieramosca, S. Hafezian, J. Gu, B. Chakraborty, D. Ballarini, L. Martinu, V. Menon, D. Sanvitto, and S. Kéna-Cohen, arXiv:1803.4352.

[59] T. C. H. Liew, A. V. Kavokin, and I. A. Shelykh, Phys. Rev. Lett. **101**, 016402 (2008).

[60] V. M. Menon, L. I. Deych, and A. A. Lisyansky, Nat. Photon. **4**, 345 (2010).

[61] A. Amo, T. C. H. Liew, C. Adrados, R. Houdré, E. Giacobino, A. V. Kavokin, and A. Bramati, Nat. Photon. **4**, 361 (2010).